Ratchet transport powered by chiral active particles

Bao-quan Ai[1,*]

[1]Guangdong Provincial Key Laboratory of Quantum Engineering and Quantum Materials, School of Physics and Telecommunication Engineering, South China Normal University, Guangzhou 510006, China
[*]corresponding. aibq@scnu.edu.cn

arXiv:1612.08174v1 [cond-mat.soft] 24 Dec 2016

ABSTRACT

We numerically investigate the ratchet transport of mixtures of active and passive particles in a transversal asymmetric channel. A big passive particle is immersed in a 'sea' of active particles. Due to the chirality of active particles, the longitudinal directed transport is induced by the transversal asymmetry. For the active particles, the chirality completely determines the direction of the ratchet transport, the counterclockwise and clockwise particles move to the opposite directions and can be separated. However, for the passive particle, the transport behavior becomes complicated, the direction is determined by competitions among the chirality, the self-propulsion speed, and the packing fraction. Interestingly, within certain parameters, the passive particle moves to the left, while active particles move to the right. In addition, there exist optimal parameters(the chirality, the height of the barrier, the self-propulsion speed and the packing fraction) at which the rectified efficiency takes its maximal value. Our findings could be used for the experimental pursuit of the ratchet transport powered by chiral active particles.

Introduction

Active matter is a rapidly growing branch of nonequilibrium soft matter physics with relevance to chemistry, biology, and complex systems.[1,2] Self-propelled particles are assumed to have an internal propulsion mechanism, which may use energy from an external source and transform it under nonequilibrium conditions into the directed motion. Compared with passive particles, active particles moving in confined structures could exhibit peculiar behaviors,[3–45] resulting for example in collective motion in complex systems,[3,4] spontaneous rectified transport,[5–17] separation of active particles based on their swimming properties,[18–25] phase separation of self-propelled particles,[26–30] trapping of particles in the microwedge,[31] spiral vortex formation in the circular confinement,[32] depletion of elongated particles from low-shear regions,[33] and the other interesting transport phenomena.[34–45]

More recently, ratchet effects have been observed in the absence of an external drive for systems of self-propelled particles.[5] Experimental studies[6–8] show the key role of self-propulsion for rectifying cell motion in an array of asymmetric funnels[6] or for driving a nano-sized ratchet-shaped wheel.[7] There also has been increasing interest in theoretical work on the rectification of self-propelled particles.[9–17] The rectification phenomenon of overdamped swimming bacteria was theoretically observed in a system with an array of asymmetric barriers.[9] In a compartmentalized channel, Ghosh and co-workers[10,11] studied the transport of Janus particles and found that the rectification can be orders of magnitude stronger than that for ordinary thermal potential ratchets. Angelani and co-workers[12] studied the run-and tumble particles in periodic potentials and found that the asymmetric potential produces a net drift speed. Potosky and co-workers[14] found that the spatially modulated self-propelled velocity can induce the directed transport.

In nature and technology, many systems are mixtures of different particle types. Studying and comparing the passive and active motions can provide insight into out-of-equilibrium phenomena.[46,47] In this paper, we numerically study the directed transport of mixtures of active and passive particles in a transversal asymmetric channel, where the big passive is immersed in the 'sea' of active particles. We emphasize on finding how the transversal asymmetry induces the longitudinal directed transport and how interactions from the 'sea' of active particles trigger the ratchet transport of the passive particle.

Model and methods

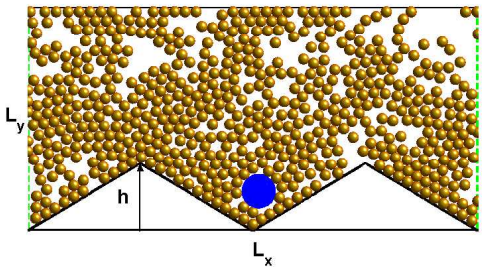

Figure 1. (Color online) Schematic of chirality-powered motor. A M-shaped barrier is regularly arrayed at the bottom of the channel. Periodic boundary conditions are imposed in the *x*-direction, and hard wall boundaries in the *y*-direction. The small gold balls denote active particles and the big blue ball denotes the passive particle.

We consider the mixtures of the passive and active particles moving in a two-dimensional channel with hard walls (the height L_y) in the *y*-direction and periodic boundary con-

ditions (the period L_x) in the x-direction (shown in Fig. 1). A M-shape barrier with the height h is regularly arrayed at the bottom of the channel. A big passive particle (blue ball) is immersed in a 'sea' of clockwise (or counterclockwise) particles(gold balls). The dynamics of particle i are described by the position $\mathbf{r}_i \equiv (x_i, y_i)$ of its center and the orientation θ_i of the polar axis $\hat{\mathbf{n}}_i \equiv (\cos\theta_i, \sin\theta_i)$. The i-th particle has radius a_i ($a_i = a_0$ for active particles and $a_i = a_p$ for the passive particle). The particle i obeys the following overdamped Langevin equations[24,38]

$$\partial_t \mathbf{r}_i = v_i^0 \hat{\mathbf{n}}_i + \mu \sum_{j \neq i} \mathbf{F}_{ij} + \sqrt{2D_0}\xi_i^T(t), \tag{1}$$

$$\partial_t \theta_i = \Omega + \sqrt{2D_\theta}\xi_i(t), \tag{2}$$

with μ the mobility and v_i^0 the self-propulsion speed ($v_i^0 = v_0$ for active particles and $v_i^0 = 0$ for the passive particle). The translational and rotational noise terms, $\xi_i^T(t)$ and $\xi_i(t)$ are Gaussian white noises with zero mean and correlations $\langle \xi_{i\alpha}^T(t)\xi_{j\beta}^T(s)\rangle = \delta_{ij}\delta_{\alpha\beta}\delta(t-s)$ (α, β labels denote Cartesian coordinates)and $\langle \xi_i(t)\xi_j(s)\rangle = \delta_{ij}\delta(t-s)$. $\langle ...\rangle$ denotes an ensemble average over the distribution of noise and δ the Dirac delta function. D_0 and D_θ denote the translational and rotational diffusion coefficients, respectively. Ω is the angular velocity and its sign determines the chirality of active particles. We define particles as the clockwise particles for negative Ω and the counterclockwise particles for positive Ω.

The force $\mathbf{F}_{ij}$ between particles i and j is assumed to be of the linear spring form with the stiffness constant k: $\mathbf{F}_{ij} = F_{ij}\hat{\mathbf{r}}_{ij}$, with $\hat{\mathbf{r}}_{ij} = (\mathbf{r}_i - \mathbf{r}_j)/r_{ij}$, $r_{ij} = |\mathbf{r}_i - \mathbf{r}_j|$, and $F_{ij} = k(a_i + a_j - r_{ij})$ if $r_{ij} < a_i + a_j$ and $F_{ij} = 0$ otherwise. The interactions between particles are radially symmetric and do not directly coupled to angular dynamics. We define the ratio between the area occupied by particles and the total available area as the packing fraction $\phi = \sum_{i=1}^N \pi a_i^2/(L_x L_y - \frac{1}{2}L_x h)$, where N is the total number of particles. For the high packing fraction ϕ in excess of 1, particles of either species overlap on average.

Eqs.(1,2) can be rewritten in the dimensionless forms by introducing characteristic length scale and time scale: $\hat{\mathbf{r}} = \frac{\mathbf{r}}{a_0}$, $\hat{t} = \mu k t$,

$$\partial_{\hat{t}} \hat{\mathbf{r}}_i = \hat{v}_i^0 \hat{\mathbf{n}}_i + \sum_{j \neq i} \hat{\mathbf{F}}_{ij} + \sqrt{2\hat{D}_0}\hat{\xi}_i^T(\hat{t}), \tag{3}$$

$$\partial_{\hat{t}} \theta_i = \hat{\Omega} + \sqrt{2\hat{D}_\theta}\hat{\xi}_i(\hat{t}), \tag{4}$$

and the other parameters can be rewritten as $\hat{v}_0 = \frac{v_0}{\mu k a_0}$, $\hat{\Omega} = \frac{\Omega}{\mu k}$, $\hat{D}_\theta = \frac{D_\theta}{\mu k}$, $\hat{D}_0 = \frac{D_0}{\mu k a_0^2}$, $\hat{a}_p = \frac{a_p}{a_0}$, $\hat{L}_{x,y} = \frac{L_{x,y}}{a_0}$, and $\hat{h} = \frac{h}{a_0}$. From now on, we will use only dimensionless variables and shall omit the hat for all quantities occurring in the above equations.

The behaviors of quantities of interest can be corroborated by Brownian dynamic simulations performed by the integration of Langevin equations(3,4). We only consider the x-direction average velocity because particles are confined in the y-direction. The average velocity along the x-direction in the asymptotic long-time regime can be obtained from the formula $\langle V_x\rangle = \frac{1}{N}\sum_{i=1}^N \lim_{t\to\infty} \frac{[x_i(t) - x_i(0)]}{t}$. We define the scaled average velocity $V_s = \langle V_x\rangle / v_0$ for convenience.

Results and Discussion

For numerical simulations, the total integration time was more than 10^7 and the transient effects were estimated and subtracted. The integration step time Δt was chosen to be smaller than 10^{-4}. With these parameters, the simulation results are robust. Unless otherwise noted, our simulations are under the parameter sets: $D_0 = 10^{-4}$, $D_\theta = 5 \times 10^{-4}$, $L_x = 40.0$, $L_y = 20.0$, and $a_p = 3.0$.

As we know, in nonlinear systems, the ratchet setup demands two key ingredients[48] which are (a)Fluctuating input zero-mean force: it should break the thermodynamical equilibrium, which forbids appearance of the directed transport due to the Second Law of Thermodynamics. (b)Asymmetry (temporal and/or spatial): it can violate the left-right symmetry of the response. For our system, the term $v_0 \cos\theta$ in Eq.(1) can be seen as the fluctuating input zero-mean force and the asymmetry comes from the upper-lower asymmetry of the channel. Now we will discuss how the chirality of active particles breaks the thermodynamical equilibrium and induces the ratchet transport.

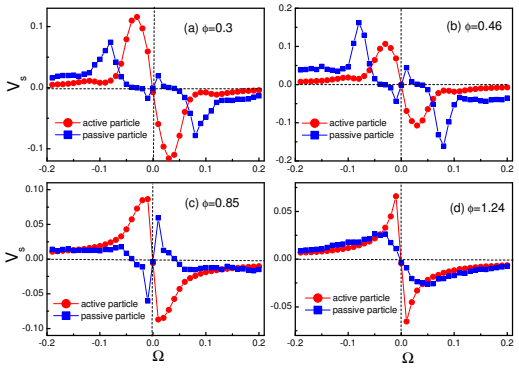

Figure 2. (Color online) Average velocity V_s as a function of the angular velocity Ω. (a)$\phi = 0.3$. (b)$\phi = 0.46$. (c)$\phi = 0.85$. (d)$\phi = 1.24$. The other parameters are $v_0 = 0.5$ and $h = 10.0$.

Figure 2 shows the average velocity V_s as a function of the angular velocity Ω for different values of ϕ. For active particles (denoted by the red lines), V_s is negative for $\Omega > 0$, zero at $\Omega = 0$, and positive for $\Omega < 0$. The movement direction of active particles is completely determined by the sign of Ω. In other words, active particles with different chiralities move to different directions and can be separated. In addition, when $|\Omega| \to \infty$, the self-propelled angle changes very fast, particles will experience a zero averaged force, so V_s tends to zero.

Therefore, there exists an optimal value of $|\Omega|$ at which $|V_s|$ takes its maximal value.

Now we explain the rectified mechanism of chiral active particles in the upper-lower asymmetric channel(see Fig. 3). In a wide channel, if the channel cell is large enough and no external perturbations, chiral active particles will perform the circular motion and repeat it and the radius of the circular trajectory is about $v_0/|\Omega|$. However, in our system, the radius of the circular trajectory is much larger than the channel cell and chiral particles can not perform circular motion. Due to the confinement of the channel, particles slide along the walls. For the clockwise particles ($\Omega < 0$) shown in Fig. 3, due to the upper-lower asymmetry of the channel, the motion time along the lower wall is significantly larger than along the upper wall, therefore, the clockwise particles on average move to the right. In a similar way, the counterclockwise particles ($\Omega > 0$) will on average move to the left.

For the single passive particle, the ratchet effect disappears ($V_s = 0$) due to the absence of the fluctuating input zero-mean force. However, when the passive particle was immersed in the 'sea' of active particles, the interactions from active particles can break the thermodynamical equilibrium and make the passive particle move directionally. At the high packing fraction (e. g. $\phi = 1.24$ shown in Fig. 2(d)), the passive and active particles have the similar transport behaviors. This is because the passive particle is completely controlled by chiral active particles at the high packing fraction. However, when $\phi < 1.0$, the ratchet behaviors of the passive particle (blue lines) are different from those of active particles (red lines). Interestingly, for very small values of $|\Omega|$ (e. g. $|\Omega| = 0.01$), the passive and active particles move to the opposite directions. Since the transport behavior powered by the counterclockwise particles is completely opposite to that powered by the clockwise particles, we only consider the case of the clockwise particles ($\Omega < 0$) in the following discussion.

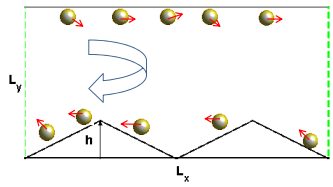

Figure 3. (Color online)Sketch of the rectified mechanism of clockwise particles in the upper-lower asymmetric channel.

In Fig. 4 we present the average velocity V_s as a function of the self-propulsion speed v_0 for both active and passive particles. For the case of active particles (see the red lines in Fig. 4), all curves are observed to be bell shaped, and there exists an optimal value of v_0 at which V_s takes its maximal value. When v_0 tends to zero, the fluctuating input disappears and the ratchet effect disappears, thus V_s is nearly equal to zero. For very large values of v_0, the chirality of the particle can be negligible, the left-right symmetry can not be broken and the directed transport gradually disappears. Therefore, the optimal self-propulsion speed can facilitate the rectification of active particles. As $|\Omega|$ increases, the position of the peak shifts to the large values of v_0.

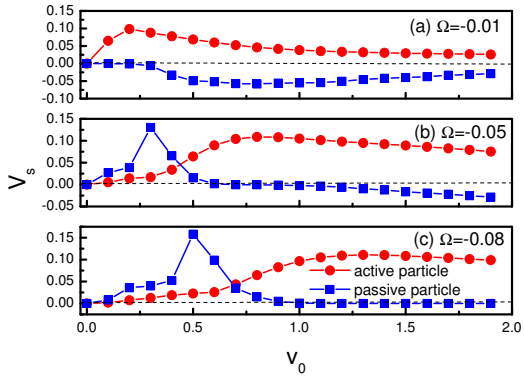

Figure 4. (Color online) Average velocity V_s as a function of the self-propulsion speed v_0 for both active and passive particles. (a)$\Omega = -0.01$. (b)$\Omega = -0.05$. (c)$\Omega = -0.08$. The other parameters are $\phi = 0.46$ and $h = 10.0$.

For the case of the passive particle (see the blue lines in Fig. 4), the transport behavior becomes complicated. Similar to Figs. 2(a)-2(c), current reversals occur for the case of very small value of $|\Omega|$ (e. g. $\Omega = -0.01$). The average velocity is always positive for the case of $\Omega = -0.08$. Interestingly, for the case of $\Omega = -0.05$, the passive particle moves to the right for $v_0 < 1.0$ and the left for $v_0 > 1.0$. Therefore, the self-propulsion speed can also determine the movement direction of the passive particle.

The dependence of the average velocity V_s on the height h of the M-shaped barrier is shown Fig. 5. For both passive and active particles, all curves are observed to be bell shaped, and there exists an optimal value of h at which $|V_s|$ takes its maximal value. When $h \to 0$, the asymmetry will disappear and no directed transport occurs. For very large values of h, the channel is blocked, particles cannot pass through the M-shape barrier, thus v_s tends to zero. Therefore, the optimal height can facilitate the ratchet transport.

Figure 6 shows the average velocity V_s as a function of the packing fraction ϕ for both active and passive particles. For the case of active particles (see the red lines in Fig. 6), the average velocity V_s is a peaked function of ϕ. We will then explain this behavior. The interactions between particles can cause two results: (A) reducing the self-propelled

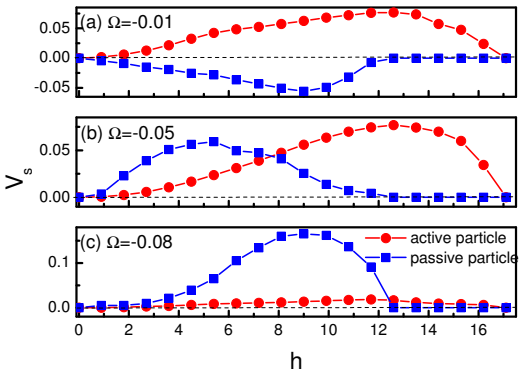

Figure 5. (Color online)Average velocity V_s as a function of the height h of the M-shaped barrier for both active and passive particles. (a)$\Omega = -0.01$. (b)$\Omega = -0.05$. (c)$\Omega = -0.08$. The other parameters are $\phi = 0.46$ and $v_0 = 0.5$.

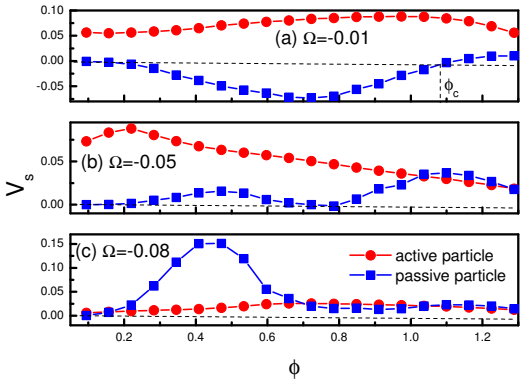

Figure 6. (Color online) Average velocity V_s a function of the packing fraction ϕ for both active and passive particles. (a)$\Omega = -0.01$. (b)$\Omega = -0.05$. (c)$\Omega = -0.08$. The other parameters are $v_0 = 0.5$ and $h = 10.0$.

driving, which blocks the ratchet transport and (B)activating motion in an analogy with the thermal noise activated motion for a single stochastically driven ratchet, which facilitates the ratchet transport. When the packing fraction increases from zero, the factor B first dominates the transport, so the average velocity increases with the packing fraction. However, when the packing faction become large, the factor A dominates the transport, thus the average velocity decreases with increasing ϕ. Therefore, there exists an optimal value of ϕ at which the average velocity is maximal.

For the passive particle ((see the blue lines in Fig. 6), the transport behavior (V_s vs ϕ) becomes more complicated. When $|\Omega| > 0.05$ (e. g. $\Omega = -0.08$), V_s is positive and there exist two peaks in the curve. For very small values of $|\Omega|$ (e. g. $\Omega = -0.01$), V_s is negative for $\phi < \phi_c$, zero at $\phi = \phi_c$, and positive for $\phi > \phi_c$. Therefore, we can also have current reversals by changing the packing fraction.

Concluding remarks

In conclusion, we numerically studied the transport of mixtures of active and passive particles moving in a periodic channel with a M-shaped barrier. A big passive particle was immersed in the 'sea' of active particles. The longitudinal ratchet transport of particles can be induced by the transversal asymmetry. The interactions from chiral active particles can make the passive particle move directionally. For active particles, the direction of the ratchet transport is completely determined by the chirality of active particles, the average velocity is positive for $\Omega < 0$, zero at $\Omega = 0$ and negative for $\Omega > 0$. In other words, the counterclockwise and clockwise particles move to the opposite directions and can be separated. However, the transport behavior of the passive particle becomes complicated, the direction of the ratchet transport is determined by competitions among the chirality, the self-propulsion speed, and the packing fraction. Remarkably, within certain parameters, the passive and active particles move to the opposite directions, for example, the big passive particle moves to the left, while active particles move to the right when $\Omega = -0.01$ and $\phi < 1.0$. We also found that there exist optimal parameters (the chirality, the height of the barrier, the self-propulsion speed and the packing fraction) at which the average velocity takes its maximal value.

Our results should be of considerable practical and theoretical interest, because they provide new insights into active matter and non-equilibrium systems. Applications of these results can be envisioned for ion mixtures traveling through cell membranes or moving through artificial nanopores, for the controlling transport in colloidal suspensions, and for the particle separation.

References

1. Marchetti, M. C. *et al*. Hydrodynamics of soft active matter. *Rev. Mod. Phys.* **85**, 1143 (2013).

2. Elgeti, J., Winkler, R. G., Gompper, G. Physics of microswimmers-single particle motion and collective behavior: a review. *Rep. Prog. Phys.* **78**, 056601(2015).

3. Vicsek, T. & Zafeiris, A. Collective motion. *Phys. Rep.* **517**,71-140 (2012).

4. Nepusz, T. & Vicsek, T. Controlling edge dynamics in complex networks. *Nature Phys*. **8**, 568-573(2012).

5. Cates, M. E. Diffusive transport without detailed balance in motile bacteria: does microbiology need statistical physics?. *Rep. Prog. Phys.* **75**, 042601(2012).

6. Galajda, P., Keymer, J., Chaikin, P. & Austin, R. A Wall of Funnels Concentrates Swimming Bacteria. *J. Bacteriol*. **189**, 8704-8707(2007).

7. Leonardo, R. D. *et al*. Bacterial ratchet motors. *Proc. Natl Acad. Sci. USA* **107**, 9541-9545(2010).

8. Kaiser, A. *et al*. Transport Powered by Bacterial Turbulence. *Phys. Rev. Lett*. **112**, 158101(2014).

9. Wan, M. B., Olson Reichhardt, C. J., Nussinov, Z. & Reichhardt, C. Rectification of Swimming Bacteria and Self-Driven Particle Systems by Arrays of Asymmetric Barriers. *Phys. Rev. Lett*. 101, 018102 (2008).

10. Ghosh, P. K., Misko, V. R., Marchesoni, F. & Nori, F. Self-Propelled Janus Particles in a Ratchet: Numerical Simulations. *Phys. Rev. Lett*. **110**, 268301 (2013).

11. Ghosh, P. K., Li, Y., Marchesoni, F. & Nori, F. Pseudochemotactic drifts of artificial microswimmers. *Phys. Rev. E* **92**, 012114 (2015).

12. Angelani, L., Leonardo, R. D. & Ruocco, G. Self-Starting Micromotors in a Bacterial Bath. *Phys. Rev. Lett*. **102**, 048104 (2009).

13. Maggi,C., Marconi, U. M. B., Gnan, N. & Leonardo, R. D. Multidimensional stationary probability distribution for interacting active particles. *Sci. Rep.* **5**, 10742(2015).

14. Pototsky, A., Hahn, A. M. & Stark, H. Rectification of self-propelled particles by symmetric barriers. *Phys. Rev. E* **87**, 042124 (2013).

15. Potiguar, F. Q., Farias, G. A. & Ferreira, W. P. Self-propelled particle transport in regular arrays of rigid asymmetric obstacles. *Phys. Rev. E* **90**, 012307 (2014).

16. Guidobaldi, A. *et al*. Geometrical guidance and trapping transition of human sperm cells. *Phys. Rev. E* **89**, 032720 (2014).

17. Koumakis, N., Maggi,C. & Leonardo, R. D. Directed transport of active particles over asymmetric energy barriers. *Soft Matter* **10**, 5695(2014).

18. Costanzo, A. *et al*. Motility-sorting of self-propelled particles in microchannels. *EPL* **107**, 36003(2014).

19. Ai, B. Q., He, Y. F. & Zhong, W. R. Chirality separation of mixed chiral microswimmers in a periodic channel. *Soft Matter* **11**, 3852-3859(2015).

20. Maggi, C. *et al*. Motility fractionation of bacteria by centrifugation. *Soft Matter* **9**, 10885-10890(2013).

21. Yang, W. *et al*. Using self-driven microswimmers for particle separation. *Soft Matter* **8**, 5175-5179(2012).

22. McCandlish, S. R., Baskarana, A. & Hagan, M. F. Spontaneous segregation of self-propelled particles with different motilities. *Soft Matter* **8**, 2527-2534(2012).

23. Berdakin, I. *et al*. Influence of swimming strategy on microorganism separation by asymmetric obstacles. *Phys. Rev. E* **87**, 052702(2013).

24. Mijalkov, M. & Volpe, G. Sorting of chiral microswimmers. *Soft Matter* **9**, 6376-6381(2013).

25. Reichhardt, C. & Olson Reichhardt, C. J. Active matter ratchets with an external drift. *Phys. Rev. E* **88**, 062310 (2013).

26. Buttinoni, I. *et al*. Dynamical Clustering and Phase Separation in Suspensions of Self-Propelled Colloidal Particles. *Phys. Rev. Lett.* **110**, 238301 (2013).

27. Schwarz-Linek, J. *et al*. Phase separation and rotor self-assembly in active particle suspensions. *Proc. Natl Acad. Sci. USA* **109**, 4052-4057(2012).

28. Stenhammar, J., Marenduzzo, D., Allen, R. J. & Cates, M. E. Phase behaviour of active Brownian particles: the role of dimensionality. *Soft Matter* **10**, 1489-1499(2014).

29. Fily, Y. & Marchetti, M. C. Athermal Phase Separation of Self-Propelled Particles with No Alignment. *Phys. Rev. Lett*. **108**, 235702(2012).

30. Stenhammar, J., Wittkowski, R., Marenduzzo, D. & Cates, M. E. Activity-Induced Phase Separation and Self-Assembly in Mixtures of Active and Passive Particles. *Phys. Rev. Lett*.**114**, 018301 (2015).

31. Kaiser, A., Wensink, H. H. & Löwen, H. How to Capture Active Particles. *Phys. Rev. Lett*.**108**, 268307 (2012).

32. Wioland, H. *et al*. Con?nement stabilizes a bacterial suspension into a spiral vortex. *Phys. Rev. Lett*.**110**, 268102 (2013).

33. Rusconi, R., Guasto, J. S. & Stocker, R. Bacterial transport suppressed by fluid shear. *Nature Phys.* **10**, 212(2014).

34. Hagen, B. T. *et al*. Gravitaxis of asymmetric self-propelled colloidal particles. *Nat. Commun*. **5**, 4829(2014).

35. Peruani, F., Klauss, T., Deutsch, A. & Voss-Boehme A. Traffic Jams, Gliders, and Bands in the Quest for Collective Motion of Self-Propelled Particles. *Phys. Rev. Lett*. **106**, 128101 (2011).

36. Hagen, B. T., Wittkowski, R. & Löwen, H. Brownian dynamics of a self-propelled particle in shear flow. *Phys. Rev. E* **84**, 031105(2011).

37. Ao, X. *et al*. Diffusion of chiral Janus particles in a sinusoidal channel. *EPL* **109**, 10003 (2015).

38. Volpe, G., Gigan, S. & Volpe, G. Simulation of the active Motion of a Microswimmer. *Am. J. Phys.* **82**, 659-664(2014).

39. Zhang, H. P., Beer, A., Florin, E. L. & Swinney, H. L. Collective motion and density fluctuations in bacterial colonies. *Proc. Natl Acad. Sci. USA* **107**, 13626-13630(2010).

40. Nguyen, N. H. P., Klotsa, D., Engel, M. & Glotzer, S. C. Emergent Collective Phenomena in a Mixture of Hard Shapes through Active Rotation. *Phys. Rev. Lett.* **112**, 075701 (2014).

41. DiLuzio, R. W. *et al*. Escherichia coli swim on the right-hand side. *Nature* **435**, 1271-1274 (2005).

42. Denissenko, P., Kantsler, V., Smith, D. J., Kirkman-Brown, J. Human spermatozoa migration in microchannels reveals boundary-following navigation. *Proc. Natl Acad. Sci. USA* **109**, 8007-8010(2012).

43. Li, Y., Ghosh, P. K., Marchesoni, F. & Li, B. Manipulating chiral microswimmers in a channel. *Phys. Rev. E* **90**, 062301(2014).

44. Ohta, T. & Ohkuma, T. Deformable Self-Propelled Particles. *Phys. Rev. Lett*. **102**, 154101 (2009).

45. Enculescu, M. & Stark, H. Active colloidal suspensions exhibit polar order under gravity. *Phys. Rev. Lett*. **107**, 058301 (2011).

46. Savel'ev, S., Marchesoni, F. & Nori, F. Controlling Transport in Mixtures of Interacting Particles using Brownian Motors. *Phys. Rev. Lett*. **91**, 010601 (2003).

47. Leptos, K. C. *et al*. Dynamics of Enhanced Tracer Diffusion in Suspensions of Swimming Eukaryotic Microorganisms. *Phys. Rev. Lett*. **103**, 198103 (2009).

48. Denisov, S., Hanggi, P. & Mateos, J. L. ac-driven Brownian motors: a Fokker-Planck treatment. *Am. J. Phys*. **77**, 602-606(2009).

Acknowledgements

This work was supported in part by the National Natural Science Foundation of China (Grant Nos. 11575064 and 11175067), the PCSIRT (Grant No. IRT1243), the Natural Science Foundation of Guangdong Province (Grant No. 2014A030313426), and Program for Excellent Talents at the University of Guangdong Province.

Author contributions statement

B. Q. Ai. carried out the numerical modeling and wrote the paper.

Additional information

Competing financial interests: The authors declare no competing financial interests.